NASA TN D-593

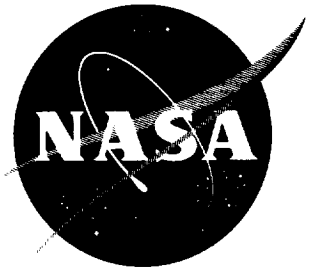

TECHNICAL NOTE
D-593

BASE-FLOW AERODYNAMICS OF A SATURN-TYPE BOOSTER STAGE AT MACH NUMBERS 0.1 TO 2.0

By John L. Allen

Lewis Research Center
Cleveland, Ohio

NATIONAL AERONAUTICS AND SPACE ADMINISTRATION
WASHINGTON
March 1962

NATIONAL AERONAUTICS AND SPACE ADMINISTRATION

TECHNICAL NOTE D-593

BASE-FLOW AERODYNAMICS OF A SATURN-TYPE BOOSTER STAGE AT MACH NUMBERS 0.1 TO 2.0

By John L. Allen

SUMMARY

The base-flow aerodynamics of an early version of the Saturn booster stage was investigated over a range of nozzle-exit to ambient static-pressure ratios up to 4.6 and stream Mach numbers from 0.1 to 2.0 using cold air in the nozzles. Base pressures were measured, as well as concentration levels of jet and exhausterator gases in the base region. The effects of base bleed and of inoperative engines were determined.

The base pressure in the center region increased linearly with nozzle pressure ratio (indicating choked outflow from the center region) for pressure ratios greater than 1.5. At the highest nozzle pressure ratio investigated, the maximum base pressure in the center region was more than twice the value in the outer-base region. Without exhausterator flow, jet-gas concentrations in the center region were as high as 100 percent (indicating choked outflow from the center region) for nozzle pressure ratios of 2.3 and higher. In the outer-base region between an outboard motor and the inner cluster, the jet-gas concentration was as high as 40 percent. Indications were that, with exhausterator flow, the concentrations of exhausterator gas in the base region were about as high as that of the jet gas without exhausterator flow. Base bleed markedly reduced the concentration of exhausterator gas in the base region. With an inboard engine inoperative, center-region base pressures decreased to about the same level as those of the outer base.

INTRODUCTION

The base heating problem observed in references 1 and 2 for missiles having single rocket motors is primarily due to recirculation of hot exhaust gases into the base region as a result of jet-stream interaction, burning of fuel-rich turbopump gases entrained in the base region, and radiation from the hot exhaust. In general, a flow model of a jet-stream interaction (ref. 3) can be used to explain the recirculation and

entrainment aspects of base heating in the atmospheric region of boost. Similar knowledge of the base-flow phenomena for multirocket bases is needed because of the current trend toward such configurations. Some of the early multirocket research (e.g., see refs. 4 to 6) has shown that, in addition to the causes of base heating described for the single jet, high heat fluxes also occur in the center of a cluster of motors because of exhaust-gas recirculation resulting from mutual impingement of the jets. A complex arrangement of eight nozzles, employing exhausterators for discharge of turbopump gases, such as for Saturn, results in several areas where mutual jet and jet-stream interactions will occur. Therefore, the following causes of base heating need to be considered:

(1) Recirculation of jet and turbopump gases into the center of the cluster due to impingement of inboard jets

(2) Flow of these hot gases from the center into the outer-base regions

(3) Recirculation of jet and turbopump exhaust gases due to impingement of outboard jets with inboard jets

(4) Recirculation of jet and turbopump exhaust gases due to the interaction of the outboard and inboard jets with the external stream

(5) Combustion of recirculated jet and fuel-rich turbopump exhaust gases

(6) Radiation from the rocket jets

Accordingly, a preliminary experimental program was undertaken in the NASA Lewis 8- by 6-foot supersonic wind tunnel to investigate the base-flow aerodynamics of an early version of the eight-rocket Saturn booster stage. Results were obtained for nozzle-exit to ambient static-pressure ratios as high as 4.6 for Mach numbers from 0.1 to 2.0 using cold air in the nozzles. In addition to base pressure measurements, concentration levels in the base region of jet and turbopump exhausts were determined by means of tracer-gas techniques.

SYMBOLS

The following symbols are used in this report:

A area

C concentration; $\frac{w_j}{w_a + w_j}$ or $\frac{w_x}{w_a + w_x}$

C_p pressure coefficient, $\frac{p - p_0}{q_0}$

D_b/D_n equivalent base to total-jet-exit diameter ratio, $\sqrt{\frac{A_b}{8A_n}}$

M Mach number

p static pressure

$p_{e,d}$ nozzle-exit pressure that results in design pressure ratio $(p_e/p_0)_d$ in tunnel

q dynamic pressure

r/r_{max} radius ratio

w weight flow

w_{bl}/w_n weight-flow ratio of bleed flow to total nozzle flow

Subscripts:

a air

b base; b,1 to b,5 denote specific locations

c specific center-star location (see fig. 2)

℄ precise center of center star

d design

e nozzle exit

j jet

n nozzle

t nozzle throat

x exhausterator

0 ambient or free stream

MODEL DETAILS, TRACER-GAS TECHNIQUE, AND INSTRUMENTATION

General Description of Model

Photographs of the 1/33-scale model of an early version of Saturn attached to the rear of a wing-mounted forebody in the transonic section of the NASA Lewis 8- by 6-foot supersonic tunnel are shown in figure 1, and schematic drawings of the principal model parts are presented in figure 2. The propellant tank cluster, engine compartment shroud, and the general base arrangement of the booster were simulated. The four axially alined inboard nozzles were spaced 0.79 nozzle-exit diameter from the base center; and the four outboard nozzles, which were canted radially outward 6°, were about 2.3 exit diameters from the center. Nozzle-exit angle was 3°. The brackets used for holding the missile on the launching pad (fig. 2) were simulated for some tests. All pertinent nozzle and base dimensions and geometric parameters are tabulated in tables I and II.

High-pressure air at a temperature of about 100° F was ducted through the wing supports to a bottlelike chamber inside the propellant tank mockup. Individual tubes for each nozzle were mounted to a bulkhead in the aft end of the air chamber, as shown in section BB of figure 2. Discharge of turbopump exhaust gases was simulated through the annular gap at each nozzle exit (fig. 2). Most of the data was obtained with the essentially flush base shown in figure 1(b) (the inner nozzles extended about 0.09 nozzle diameter from the base, and the outer nozzles about 0.13 diameter). For a portion of the test, the base plate was removed and the bulkhead served as a base surface located 4.7 exit diameters upstream of the exit plane (fig. 1(c)). This recessed-base configuration was investigated with and without a base-bleed system.

An exact simulation of base flow for rocket-motor configurations generally is not possible with cold-air jets. Simulation is particularly difficult for multinozzle configurations in the atmospheric region of boost where jet-stream interactions, as well as jet-jet interactions, occur. Accordingly, the cold-air nozzles were designed within the limits of the existing air supply such that the nozzle-exit to ambient static-pressure ratios of the full-scale hot rocket motors could be approached while maintaining the correct nozzle-exit angle and nozzle-exit to base area ratios.

The altitude - Mach number schedule anticipated for the booster and the resulting nozzle-exit to ambient pressure ratio are shown in figure 3. As shown in the figure, the altitude limits of the tunnel were somewhat less than that anticipated for the booster. As a result, the absolute value of nozzle-exit pressure for the tunnel test was about 40 percent greater than the value for the booster in order to maintain approximately the correct exit-to-ambient design pressure ratio schedule

$(p_e/p_0)_d$. The nozzle-exit pressure thus simulated at tunnel ambient pressures corresponds at the booster altitude schedule to that for a liquid-oxygen - JP-4 rocket with an area ratio of 8, at a chamber pressure of 600 pounds per square inch, an oxygen-fuel ratio of 2.4, and with one-dimensional frozen flow assumed.

In general, data were obtained over a range of flight Mach numbers for several absolute values of nozzle-exit pressure by varying the jet total pressure. For those figures where data are not presented as a function of nozzle-exit pressure ratio p_e/p_0, the data are identified in terms of the ratio of the actual to the design nozzle-exit pressure ratio $p_e/p_{e,d}$ where $p_{e,d}$ is the nozzle-exit pressure that will produce the design trajectory pressure ratio $(p_e/p_0)_d$ (fig. 3) in the tunnel. In a like manner, the exhausterator chamber pressure was maintained at several discrete absolute levels, and the data are presented in terms of the ratio $p_x/p_{e,d}$. An exhausterator flow of about 2 percent of the nozzle flow is attained for a value of $p_x/p_{e,d}$ of about 2.35.

Tracer-Gas Techniques

To determine nozzle- and exhausterator-gas concentrations in the base region, carbon dioxide was used as a tracer gas. The amount recirculating from each of the two sources was measured separately: For exhausterator concentration measurements, pure carbon dioxide was flowed through the exhausterator and pure air through the nozzle; and, for nozzle concentration measurements, carbon dioxide was added to the main nozzle air supply to produce an initial mixture ratio of about 5 percent. In the latter case, measurements were made with and without exhausterator flow of pure air. Samples from either the center of the cluster or between the inboard and outboard nozzles were pumped to an NASA mixture analyzer, which measured the percent of carbon dioxide of the sample by volume. The results were converted to percent by weight.

Instrumentation

Pressure instrumentation used for the data presented herein was principally of four general classes: (1) external pressure distribution of the engine shroud, (2) base pressure distributions, (3) nozzle-exit static pressures, and (4) exhausterator chamber pressure. The flow rates of air and CO_2 were measured separately by means of orifice meters.

The geometries and instrumentation for both the flush and recessed bases are shown in figure 4. The symbols used for the different pressure-orifice locations depict the manner chosen for presentation of the results. The solid symbols are used to compare the relative levels of the center-star and outer-base pressures, whereas the open symbols are used for base diagonal pressure distributions. The pressure tap precisely in the base center, which also served as a gas-sampling tube, was not available for all configurations. For the recessed-base configuration (fig. 4(b)), the pressure instrumentation was retained at the original plane of the base wherever possible (fig. 1(c)).

Base bleed. - Various base-bleed flow rates were obtained by removing screws from tapped ports in the recessed-base plate; this permitted high-pressure air from the air chamber to enter the base region. Since the base-bleed flow was initially at the same total pressure as that of the nozzles, bleed weight-flow ratios w_{bl}/w_n were assumed to be equal to the ratio of bleed-flow sonic area to total nozzle sonic area times a bleed-port flow coefficient of 0.7. The diameter of the bleed port in the center of the cluster was 0.250 inch, whereas all other bleed ports were 0.103 inch. The sequence in which the bleed ports were opened is shown in figure 4(b), and the bleed flow rates are given in the following table:

	w_{bl}/w_n
Center tube only	0.0056
Center tube plus 4 bleed ports	.0088
Center tube plus 8 bleed ports	.0124
Center tube plus 20 bleed ports	.023

External pressure distribution. - Pressure distributions of the engine shroud (fig. 5) are presented primarily to provide some quantitative definitions of the external flow field that enters into the stream-jet interaction; total-pressure surveys of the flow field were not made. That portion of the shroud having an initial compression surface is referred to as a lobe, whereas the expansion portion is called a valley.

The pressure coefficients at the trailing edge of the model base were slightly negative for the lobe region, and zero to slightly negative for the valley regions. Upstream of the base an expansion can be

observed where the lobe surface turns back to axial direction (fig. 2, section B-B), as well as a corresponding compression for the valley regions. These results also indicate moderating three-dimensional effects.

Installation of holddown brackets in the valleys between lobes caused an expansion to occur locally at about 3.7 inches upstream of the base (fig. 5(b)) but had little effect at the plane of the base or on lobe pressure distribution.

Changing the flow field of the tank region by covering the tanks with a cylindrical shroud had little influence on the shroud pressure distribution, and the data are not presented.

RESULTS AND DISCUSSION

Base Pressure Measurements

Because of the complex arrangement of both the nozzles and the external shroud, many different regions of the base are of interest. Therefore, base pressure data are presented in two forms: (1) pressure distribution across the base diagonal, and (2) comparison of outer and center-star base pressures.

An understanding of the main features of the base flow can be gained by first observing the base diagonal pressure distributions shown in figure 6 for the flush-base configuration. These data were obtained over a range of nozzle pressure ratio at each Mach number. At Mach 0.79 the center-star base pressures were appreciably less than those of the outer base at all nozzle pressure ratios, which indicated that the inner jets were not mutually impinging to any appreciable extent and that an aspirating effect was present. For these data the jet flow was overexpanded. At Mach 1.0 the center pressure increased, relative to outer-base pressures, as nozzle pressure ratio increased; and a fairly flat profile was achieved at $p_e/p_{e,d} = 0.925$. At higher pressure ratios, center pressures exceeded outer-base pressures, thus indicating appreciable backflow from the impingement of the inner jets toward the base surface and into the outer-base region. For all nozzle pressure ratios investigated at Mach 1.97, center pressures were much greater than those of the outer base. Outflow from the center region into the outer-base region passes between the jet boundaries upstream of the impingement point. At high nozzle pressure ratios, the center pressure may increase relative to outer-base pressure to such an extent that this outflow area will become choked. Hence, the center region would no longer be influenced by ambient or outer-base-region conditions, and the ratio of center-region base pressure to nozzle-exit pressure would be constant.

Center-star and outer-base pressure ratios are shown as a function of nozzle-exit to ambient pressure ratio in figure 7. Linear variation of the center-star pressure ratio, which was independent of stream Mach number, was obtained for nozzle-exit to ambient pressure ratios greater than about 1.5. In general, a line fairing for center-star pressures is used for the region where center-star pressure exceeds the outer-base pressure. The slope of the linear portion of this line is a constant value of p_c/p_e for choked center-star conditions, which is equal to about 0.2.

The outer-base pressures were generally uniform and were faired by a single line for constant stream Mach number. The locations of the base pressures selected for plotting are generally between a nozzle and the outer edge of the base. The pressures along the base diagonal, except for the center star, were somewhat higher than others in the outer-base region as shown in figure 6.

Comparison with single-nozzle data. - A comparison of these multinozzle results with single-nozzle data (ref. 3) is also shown in figure 7 for an equivalent base to nozzle diameter ratio, which is defined as $D_b/D_n = \sqrt{A_b/8A_n}$ for the multinozzle configuration. For a constant flight Mach number, both the multi- and single-nozzle results had the same trend with nozzle-exit to ambient pressure ratio; however, the multinozzle outer-base pressure ratios were about 25 percent lower. Considering the relatively small influence of base pressure on net missile thrust-minus-drag or base structure, single-nozzle data offer an attractive means for preliminary estimations. For this comparison the nozzle-exit Mach numbers and flight Mach numbers were 2.19 and 1.91, respectively, for the single nozzle, and 2.15 and 1.97 for the multinozzle results. Nozzle-exit angles were zero for the single nozzle, and 3° for the multinozzles. Also, the boattail angle of the single-nozzle configuration was 5.63°, whereas that for the eight-nozzle configuration was zero (although this was preceded by a flair section around the outboard nozzles and a boattail between the outboard nozzles). The effects of these minor differences are believed to be small.

Effect of holddown brackets and exhausterators. - Figure 8 shows the effects of adding missile holddown brackets and of permitting flow through the exhausterator system. Data from figure 7 are repeated for comparison purposes. With the configurations employing holddown brackets, pressures in the center of the center star $p_{\text{¢}}$ were also measured. However, center-star pressures are not presented for nozzle pressure ratios less than about 1.5 since they are lower than the outer-base pressures. In the range of linear variation of center-star base pressure with nozzle pressure ratio, the centerline pressure $p_{\text{¢}}$ was 17 to 18 percent greater than p_c with holddown brackets and 6.5 to 27 percent greater

than p_c with holddown brackets and exhausterator flow. Presumably the pressure p_{ℓ} was equal to the stagnation value of the reversed flow in the center region, whereas p_c was the local surface static pressure near the approach to one of the outflow passages. The maximum slope of the centerline pressure ratio p_{ℓ}/p_e was about 0.3. At the highest nozzle pressure ratio investigated, the centerline pressure p_{ℓ} was more than twice the base pressure measured in the outer region.

As shown by the comparison in figure 8, exhausterator flow increased the slope of the linear part of the p_{ℓ} line about 10 percent and, although not shown, the increase was nearly linear with exhausterator flow rate. The slope of the p_c line was decreased slightly by exhausterator flow and the pressure was somewhat higher than that without exhausterator flow, particularly at lower nozzle-exit to ambient pressure ratios.

The overall level of base pressure was increased by a pressure ratio of no more than 0.08 ($\Delta p/p_0$) by the holddown brackets, probably as a result of the change in Mach number and total pressure of the external flow involved in the jet-stream interaction. Results with a cylindrical cover over the cluster of propellant tanks, which are not presented, indicated an even smaller effect on base pressures.

Pressures in the outer-base region were only slightly increased by exhausterator flow, as shown in figure 8. With flow through the outboard exhausterators only, the outer-base pressure ratio was increased by a slightly larger amount; but, since the change was not significant, the data are not presented.

Effect of recessing the base and base-bleed flow. - Figure 9 presents a comparison of the base pressure for the flush-base configuration, the recessed base without bleed flow, and the recessed base with various base-bleed flow rates. Because of the increase in outflow area between the motors with the recessed base, the centerline pressures were reduced 20 percent without bleed flow. Outer-base pressures were slightly increased; however, this comparison is subject to the restriction that different base pressure locations in the outer region are being compared (see fig. 2).

The base pressure increased linearly with bleed flow rate for a given nozzle-exit to ambient pressure ratio. A bleed flow rate of 2.3 percent of the total jet flow increased the average base pressure to a value equal to, or slightly greater than, the center-star pressure that existed without bleed flow. (Since only one value of nozzle-exit to ambient pressure ratio was tested at each Mach number for the maximum bleed case, the data are identified by symbols rather than lines.) Pressure measurements in the center star were not available for the data with bleed flow.

Gas Concentration Measurements

In general, the origin of the jet flow that recirculates into the base region is the outer boundary of the jet. Thus, the recirculating flow will be rocket-exhaust gas when the exhausterators do not have flow, or exhausterator gas when they are adding a sheath of flow around the rocket exhaust. External air dilutes the recirculating gas except for the center-star region under conditions of choked outflow, and in this case the outflow presumably contributes to the flow entrained in the outer-base region. By adding a tracer gas to either the nozzle or exhausterator flow, the concentration of each in the center or outer-base regions could be measured.

Jet-gas concentrations in the base. - Measurements of the concentrations of simulated rocket-exhaust gas are shown in figure 10. As indicated in the figure, a center sample and an outer-base sample (referred to as shroud sample) were obtained. With the exhausterators turned off, the concentration in the center-star base region was 100-percent jet gas for the nozzle-exit to ambient pressure ratios greater than about 2.3, which indicated that center-region choking occurred at this and higher pressure ratios. This indication of choking occurred at a somewhat higher minimum nozzle pressure ratio than the value of 1.5 indicated by the linear variation of center pressure in figure 7. This discrepancy is probably a result of the limited accuracy of the concentration measurements. Between the inboard and outboard nozzles, the concentration was about 40 percent for nozzle-exit to ambient pressure ratios greater than about 1.2.

Turning on the pure exhausterator air would tend to shield the rocket exhaust containing the tracer gas from the mixing zone where the flow that is recirculated into the base region originates. As shown in the figure, this reduced the jet concentration to about 10 percent at either the center or shroud positions for nozzle-exit to ambient pressure ratios greater than about 2.3.

With the inboard exhausterators off, and the outboard exhausterators on, the center-region concentrations (fig. 10(a)) were essentially the same as with all the exhausterators off, as would be expected. The concentration between the inboard and outboard nozzles was about halfway between the values obtained with all exhausterators on and with all of them off (fig. 10(b)).

Only limited data were obtained with the recessed base (no bleed). Concentrations for the center-star region were essentially the same as for the flush base and are not presented.

Exhausterator-gas concentrations. - At each Mach number, exhausterator-gas concentration measurements were obtained with a nozzle pressure ratio near the design value. Since pure carbon dioxide was used as the exhausterator gas, the operating limits of the meter were such that the base-region concentrations greater than 0.32 could not be measured. (For the jet-gas concentration measurements, only 5 percent carbon dioxide was added to the jet gas, and the limit was not encountered.) Without bleed flow, as shown in table III, exhausterator-gas concentrations in the center-star position increased with nozzle pressure ratio and were at the meter limit at pressure ratios of 2.4 and higher. In the shroud position, the concentration increased with pressure ratio and reached the meter limit at the highest pressure ratio investigated.

With the recessed base and no bleed, a single center measurement was obtained. As shown in table III, the concentration was at the meter limit as with the flush base. Some reduction of gas concentration in the center due to bleed can be presumed to have occurred; however, center measurements were not possible when bleed was employed. At the shroud location the use of base bleed greatly reduced the exhausterator-gas concentration: At bleed flow ratios of 0.0124 the concentration was less than 0.04, and at a flow ratio of 0.023 the exhausterator gas could not be detected. This qualitatively agrees with the measured increase of base pressure with bleed flow, as shown in figure 9.

By comparing the data obtained with exhausterator flow through the outboard exhausterators only with that for all exhausterators in operation, the contribution of each set of exhausterators to the concentration in the center region can be determined. As expected at low nozzle pressure ratio, where a central aspirating effect was present, exhausterator gas from the outer exhausterators was detected in the center-star region. At higher pressure ratios, where outflow from the center region occurred, the outer exhausterators did not contribute to the central concentration. At the shroud location, the concentrations were comparable at low nozzle pressure ratios. However, at higher pressure ratios, the concentration progressively diminished because the gas recirculated from the outer and inner jet impingement contained only the contribution from the outer exhausterator and, in addition, the outflow of pure air from the center region diluted the concentration in the outer-base region.

Although the center-star measurements were limited by the meter to values below 32 percent, it can be argued that the concentrations should approach 100 percent. It was stated in the preceding section that, with airflow through the exhausterators and tracer gas in the nozzle flow, the concentration of jet gas in the center-star region was reduced from 100 percent to approximately 10 percent. This qualitatively illustrates that the depth or thickness of the jet boundary which recirculated into the center star as a result of the mixing process was approximately equal to the thickness of the sheath of air added to the jet boundary by the exhausterator flow. Therefore, concentrations of exhausterator gas can be expected to be about as high as those attained for jet gases without exhausterator flow. The secondary effect of the exhausterator flow

altering the expansion of the jet and the mixing process along the jet boundary must be admitted; however, the measured effect of exhausterator flow on center-star pressures amounted to an increase of less than 10 percent (fig. 8).

Effect of an Inoperative Engine on Base Pressure

Base pressure data are presented in figure 11 for the simulated condition of one inoperative outboard engine (figs. 11(a) and (b)) or one inoperative inboard engine (figs. 11(c) and (d)). Pressure distributions along the base diagonal for these conditions are shown in figure 12. For these tests it was not practical to disconnect the individual exhausterator supply lines for a particular nozzle; hence, although the jet flow of a particular nozzle was blocked off as required, its exhausterator flow was not. In order to show best the localized effects, the base pressures are plotted for two quadrants, one of which contained the inoperative nozzle.

With one outboard nozzle inoperative (figs. 11(a) and (b), and 12(a)), the outer-base pressures in the quadrant of operative engines varied less than 5 percent above or below the reference eight-nozzle data. The spread between the individual base pressures increased in the "dead engine" quadrant for nozzle-exit to ambient pressure ratios below about 3.8.

With one inoperative inboard engine (figs. 11(c) and (d), and 12(b)), the center-star pressures were reduced to the general level of outer-base pressure. Deviations from the reference eight-jet data and the increased spread between individual base pressures for the "dead engine" quadrant were about the same as those for the outboard engine-out case.

When an engine becomes inoperative in an actual multiengine rocket, the condition of primary interest occurs after the remaining engines have been gimbaled to a new stability-correcting position. Simulation of this condition was not possible with the present model.

SUMMARY OF RESULTS

Base pressure measurements for a Saturn-type booster stage using cold air in the nozzles were made over a range of nozzle-exit to ambient pressure ratios up to 4.6 at stream Mach numbers from 0.1 to 2.0. Tracer-gas techniques were employed to determine concentrations of jet gas or exhausterator gas in the base regions. The effects of various base-bleed flow rates were investigated, as well as the effects of inoperative engines. The following results were obtained:

(1) The base pressure in the center region increased linearly with nozzle-exit pressure ratio (indicating choked outflow from the center region) for nozzle pressure ratios greater than 1.5. At the highest nozzle pressure ratio investigated, the maximum base pressure in the center region was more than twice the value in the outer-base region.

(2) Without exhausterator flow, jet-gas concentrations in the center of the inner cluster were as high as 100 percent (indicating a choked outflow from the center region) for nozzle pressure ratios of about 2.3 and higher. In the region between an outboard jet and the inner cluster, the jet-gas concentration was as high as 40 percent. Similar values were obtained when the base was recessed about 4.7 nozzle-exit diameters.

(3) The use of pure air in the exhausterators reduced the jet-gas concentrations to a level of 10 to 20 percent in the center-star or outer-base regions. However, indications were that the exhausterator-gas concentration in the base was about as large as the jet-gas concentration without exhausterator flow. The use of base bleed markedly reduced the exhausterator-gas concentration in the outer-base region.

(4) Recessing the base to a depth of about 4.7 nozzle-exit diameters decreased the pressure ratio in the center of the inner cluster by about 20 percent and slightly increased the outer-base pressure ratio. Introducing various bleed flows at the recessed base gradually increased the outer-base pressures. For the maximum bleed flow rate of about 2.3 percent of the total nozzle flow, the outer-base pressures were as high or higher than no-bleed center values.

(5) Comparison of the outer-base pressure ratios with reference data for a single nozzle for an equivalent base-to-nozzle diameter ratio indicated similar trends with nozzle-to-ambient pressure ratio but at a level about 25 percent lower than that for the single-nozzle data.

(6) When one of the inner-cluster nozzles was inoperative, the pressures in the center of the cluster were reduced to the general level of those in the outer base. With one of the outboard nozzles inoperative, the center and outer-base pressures were only slightly affected.

(7) Only small effects on center or outer-base pressures were observed for changes in the external-body flow field caused by adding missile holddown brackets or changing the cluster of propellant tanks to a single cylindrical shape. Similarly, the effect of exhausterator flow on base pressures was quite small.

Lewis Research Center
National Aeronautics and Space Administration
Cleveland, Ohio, June 19, 1961

REFERENCES

1. Nettles, J. Cary: Experimental Study of Ballistic-Missile Base Heating with Operating Rocket. NACA RM E58G17, 1958.

2. Chiccine, Bruce G., Valerino, Alfred S., and Shinn, Arthur M.: Experimental Investigation of Base Heating and Rocket Hinge Moments for a Simulated Missile Through a Mach Number Range of 0.8 to 2.0. NASA TM X-82, 1959.

3. Baughman, L. Eugene, and Kochendorfer, Fred D.: Jet Effects on Base Pressures of Conical Afterbodies at Mach 1.91 and 3.12, NACA RM E57E06, 1957.

4. Scott, William R., and Slocumb, Travis H., Jr.: Jet Effects on the Base Pressure of a Cylindrical Afterbody with Multiple-Jet Exits. NASA MEMO 3-10-59L, 1959.

5. Geothert, Bernard H.: Studies of the Flow Characteristics and Performance of Multi-Nozzle Rocket Exhausts. TR 59-16, Arnold Eng. Dev. Center, Oct. 1959.

6. Grossman, R. L.: Base Heating Considerations of Multiple Rocket Nozzle Configurations. Rep. XP12.19, Grumman Aircraft Eng. Corp., Aug. 1960.

TABLE I. - NOZZLE DIMENSIONS AND AREAS

	Diameter, in.	Area, sq in.	Area ratio, A/A_t (A_t = 0.817 sq in.)
Exhausterator exit	1.41	1.56	1.91
Nozzle exit	1.394	1.525	1.87
Location of nozzle-exit statics, approx.	1.38	1.5	1.83

TABLE II. - BASE AREAS AND GEOMETRIC PARAMETERS

Total base area, sq in.	43.1
Base to nozzle area ratio, 8 nozzles	3.45
Effective diameter ratio; $\frac{D_b}{D_n} = \sqrt{\frac{A_b}{8A_n}}$	1.86
Spacing ratio = $\frac{\text{Radius to nozzle center}}{\text{Nozzle-exit radius}}$	Inboard: 1.59 Outboard: 4.62
Center-star area, sq in. Ratio of center-star to base area	0.553 .0128
Recessed-base area, sq in. Ratio of recessed to total base area	28.0 .65
Extension ratio = $\frac{\text{Distance nozzle extends}}{\text{Nozzle-exit diameter}}$	Inboard: 0.09 Outboard: .13

TABLE III. - EXHAUSTERATOR-GAS CONCENTRATIONS IN BASE REGION

Flight Mach number, M_0	Nozzle pressure ratio, p_e/p_0	Exhausterator-gas concentrations, $w_x/(w_x + w_a)$; $p_x/p_{e,d} = 2.6$						
		Flush base, no bleed		Recessed base			Closed base, outboard exhausterators only, no bleed	
		Center	Shroud	Center, $w_{bl}/w_n = 0$	Shroud, $w_{bl}/w_n = 0.0124$	Shroud, $w_{bl}/w_n = 0.023$	Center	Shroud
1.97	4.0	0.32	0.32	0.32	0.02	0	0	0.1
1.67	3.1	.32	.30	----	.02	0	0	.12
1.38	2.4	.32	.26	----	.02	0	.005	.14
1.0	1.6	----	.24	----	----	0	.005	.14
.8	1.1	.002	.08	----	.04	-	.01	.06
.09	.88	-----	----	----	----	-	.02	.007

E-901

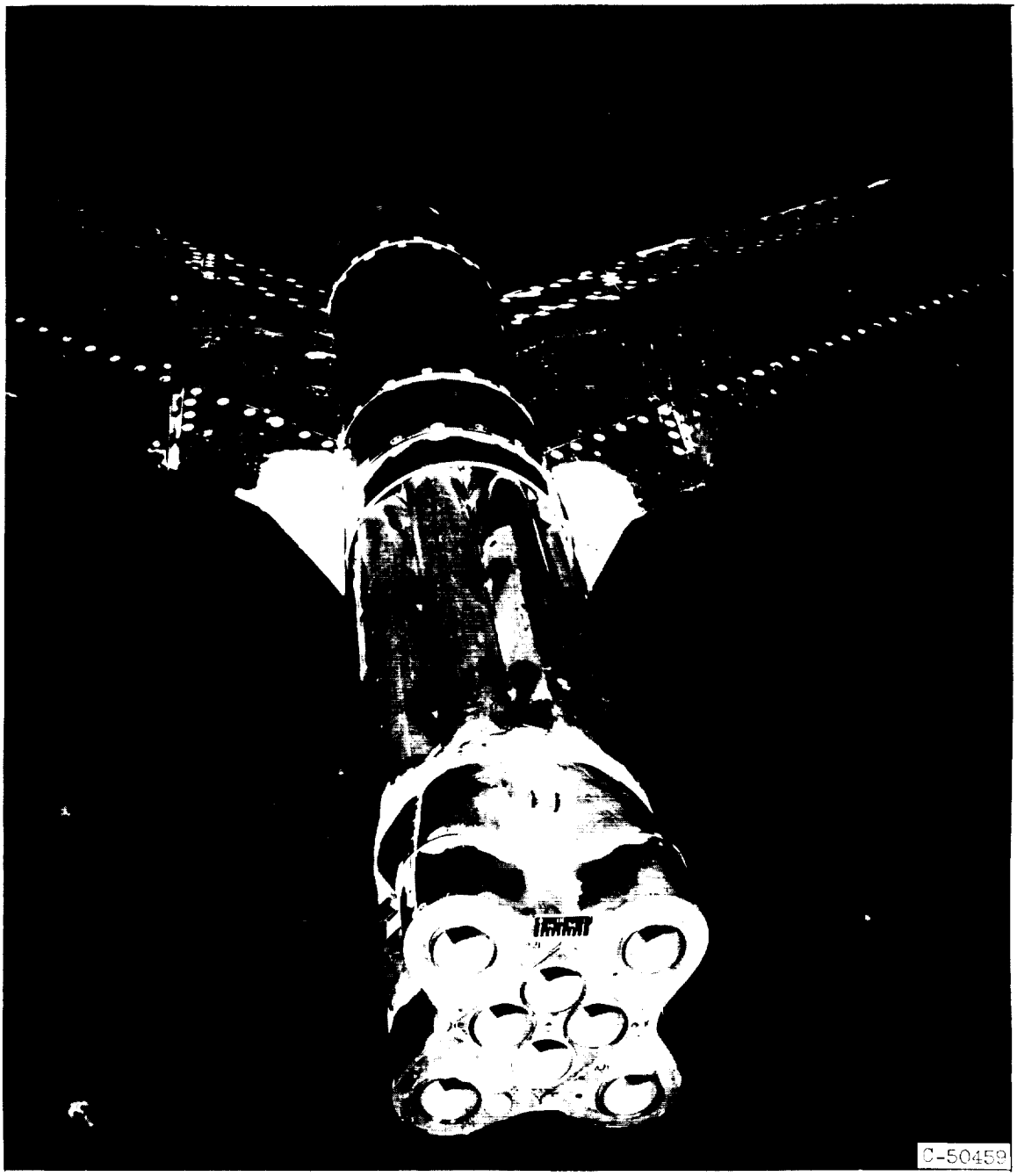

(a) 3/4 Rear view of general arrangement.

Figure 1. - 1/33-Scale model of Saturn-type booster stage.

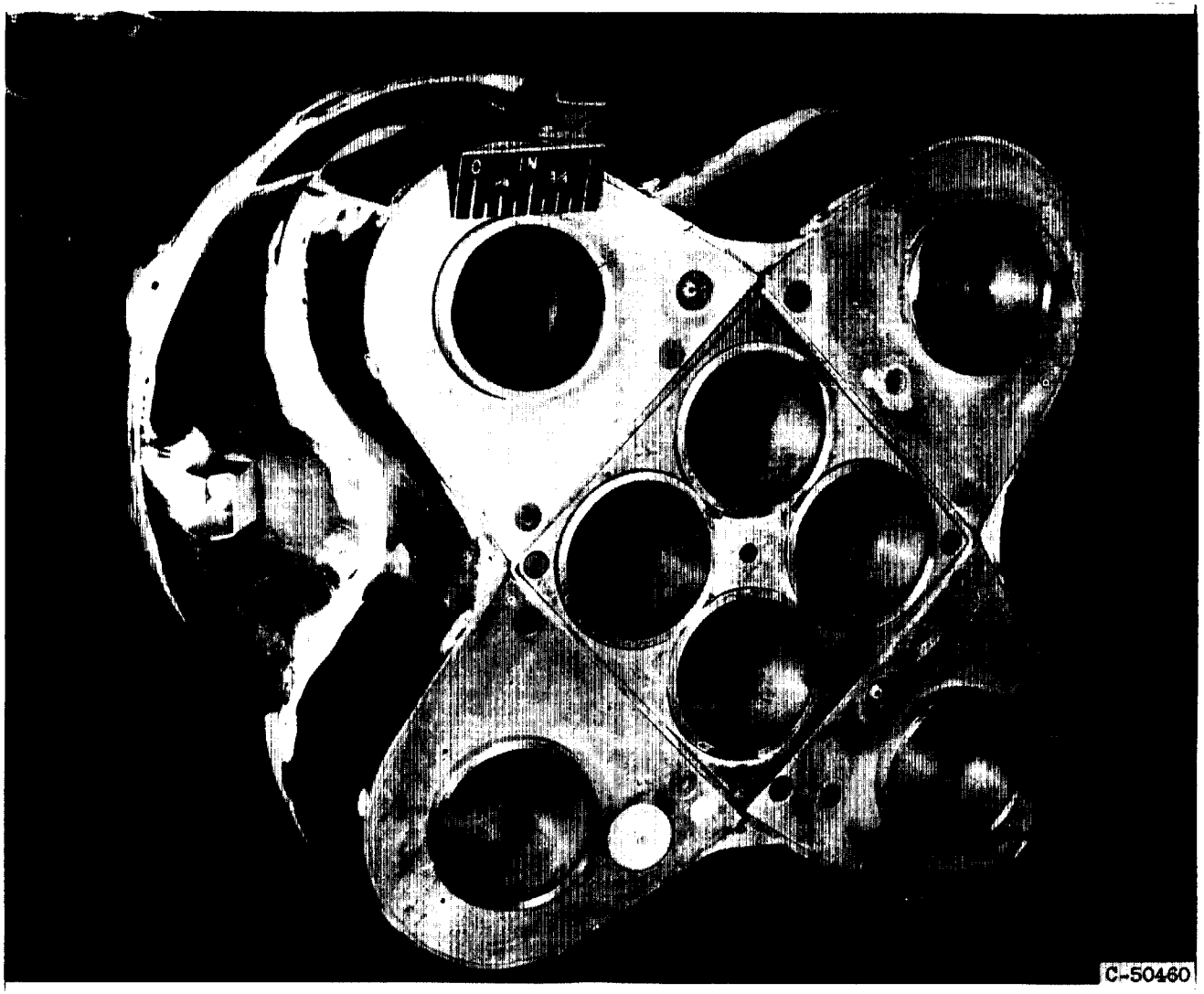

(b) Closeup of flush base.

Figure 1. - Continued. 1/33-Scale model of Saturn-type booster stage.

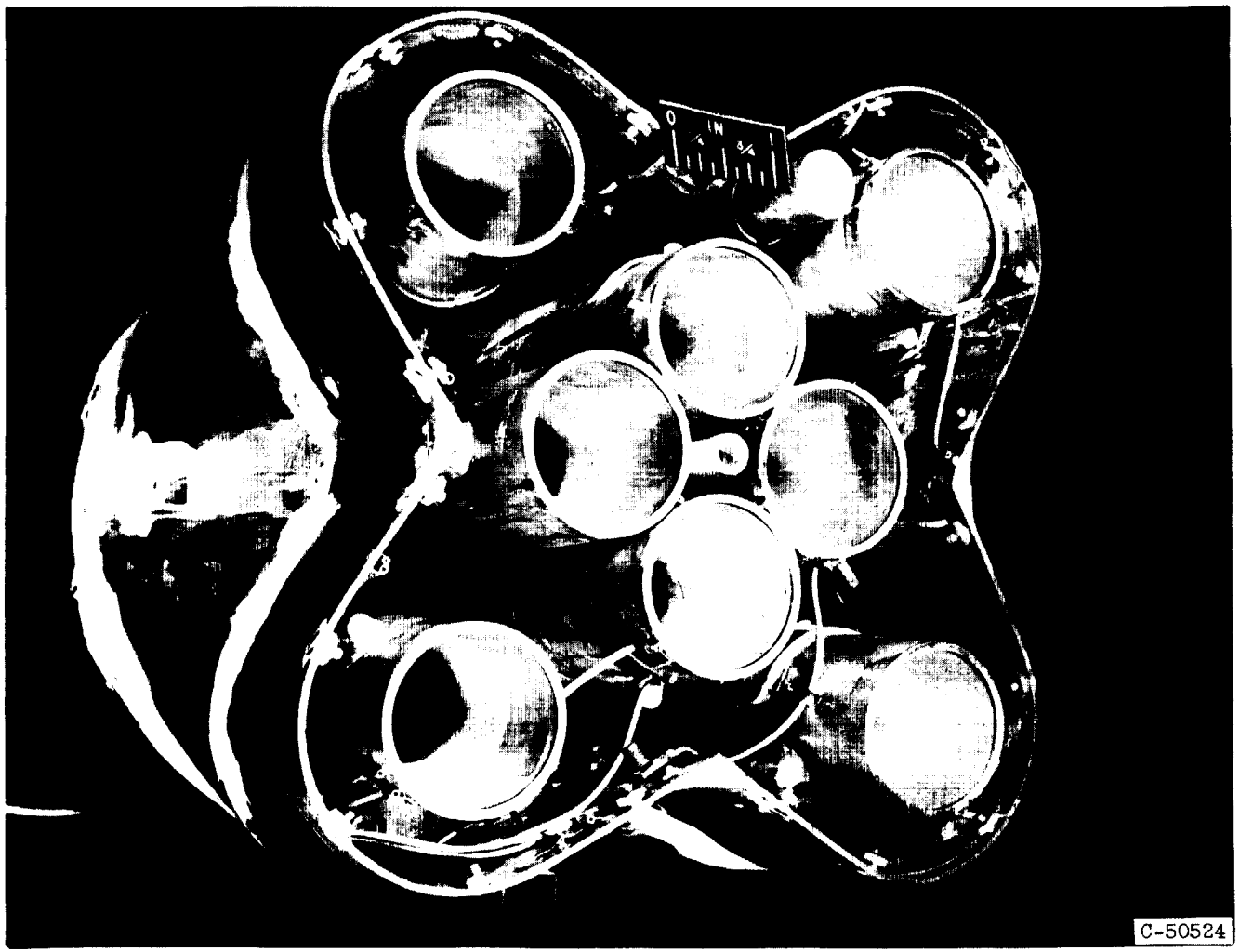

(c) Closeup of recessed base.

Figure 1. - Concluded. 1/33-Scale model of Saturn-type booster stage.

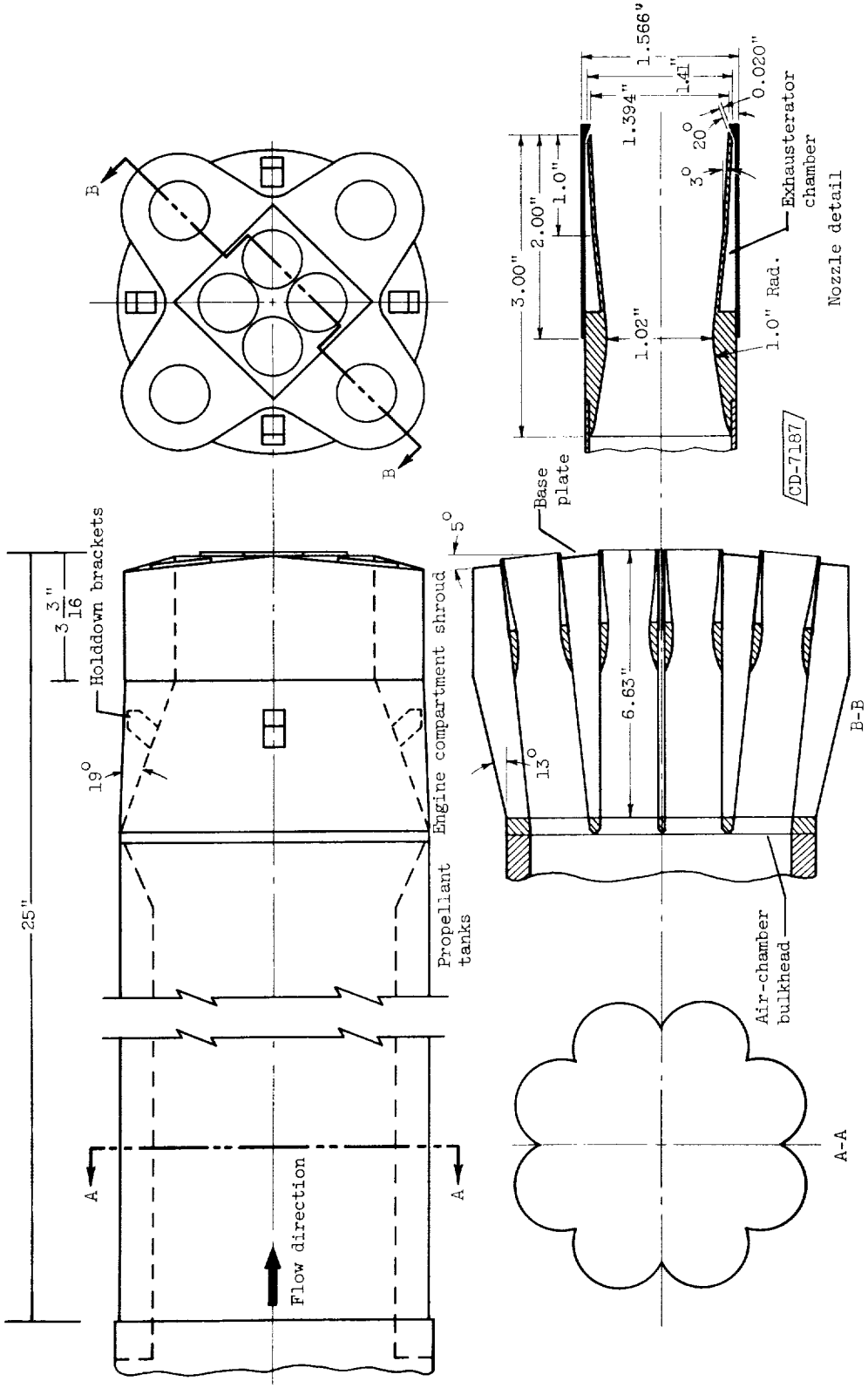

Figure 2. - Model details.

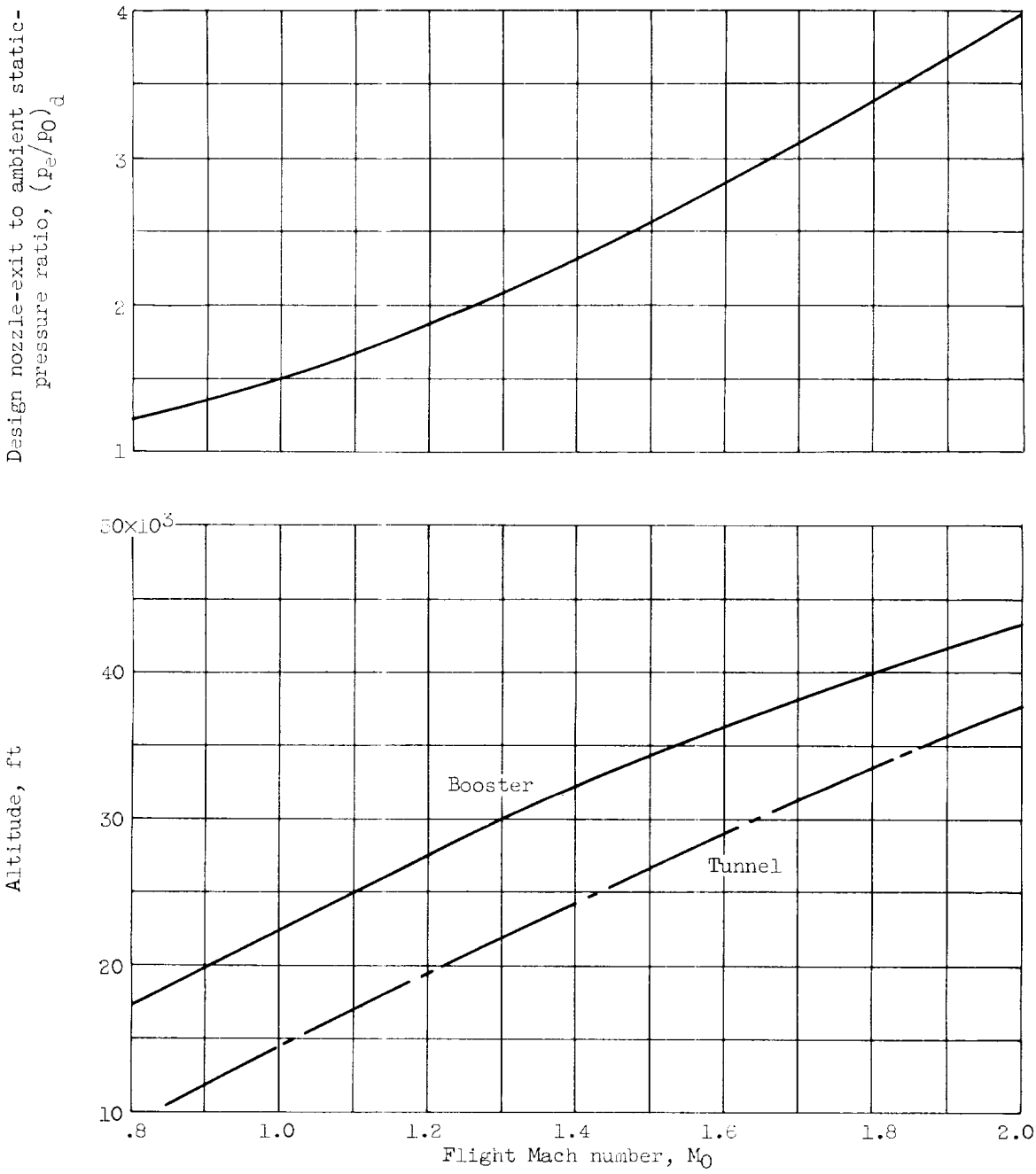

Figure 3. - Flight trajectory and corresponding nozzle-exit to ambient static-pressure ratio.

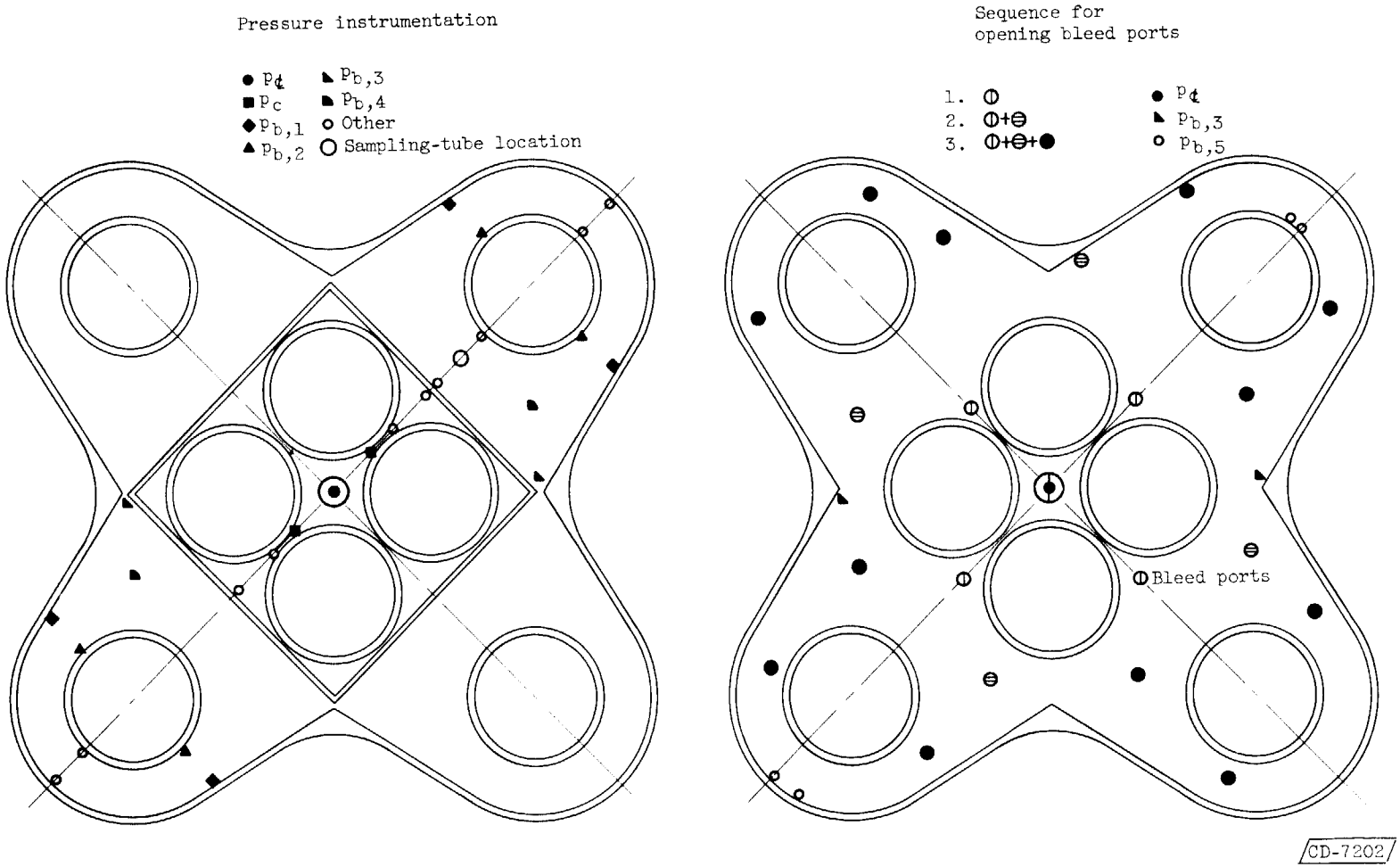

(a) Flush-base configuration.

(b) Recessed-base configuration.

Figure 4. - Base pressure instrumentation and locations of gas-sampling tubes and bleed ports.

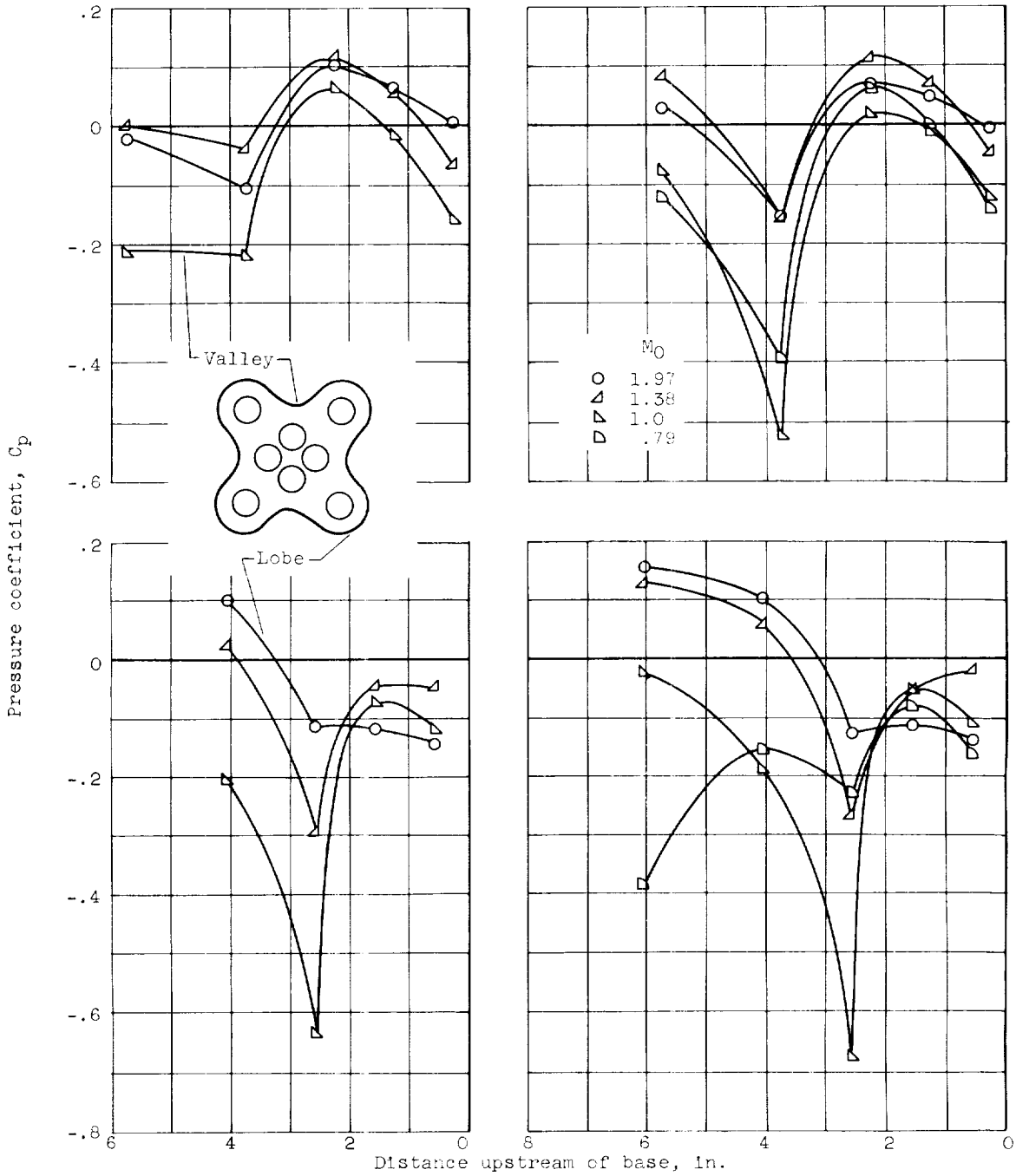

(a) Basic configuration. (b) With holddown brackets.

Figure 5. - External pressure distribution.

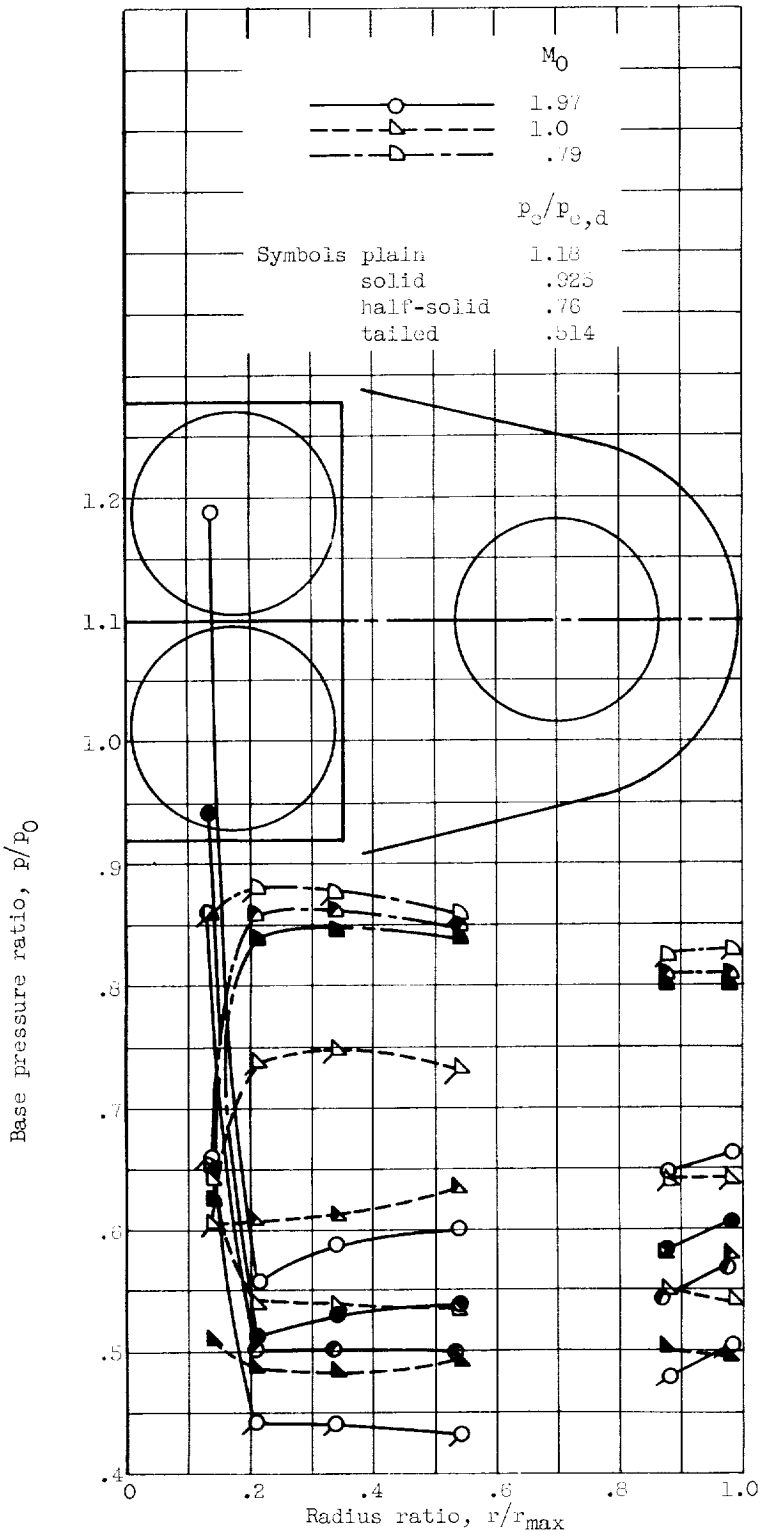

Figure 6. - Pressure distribution along base diagonal. No exhausterators.

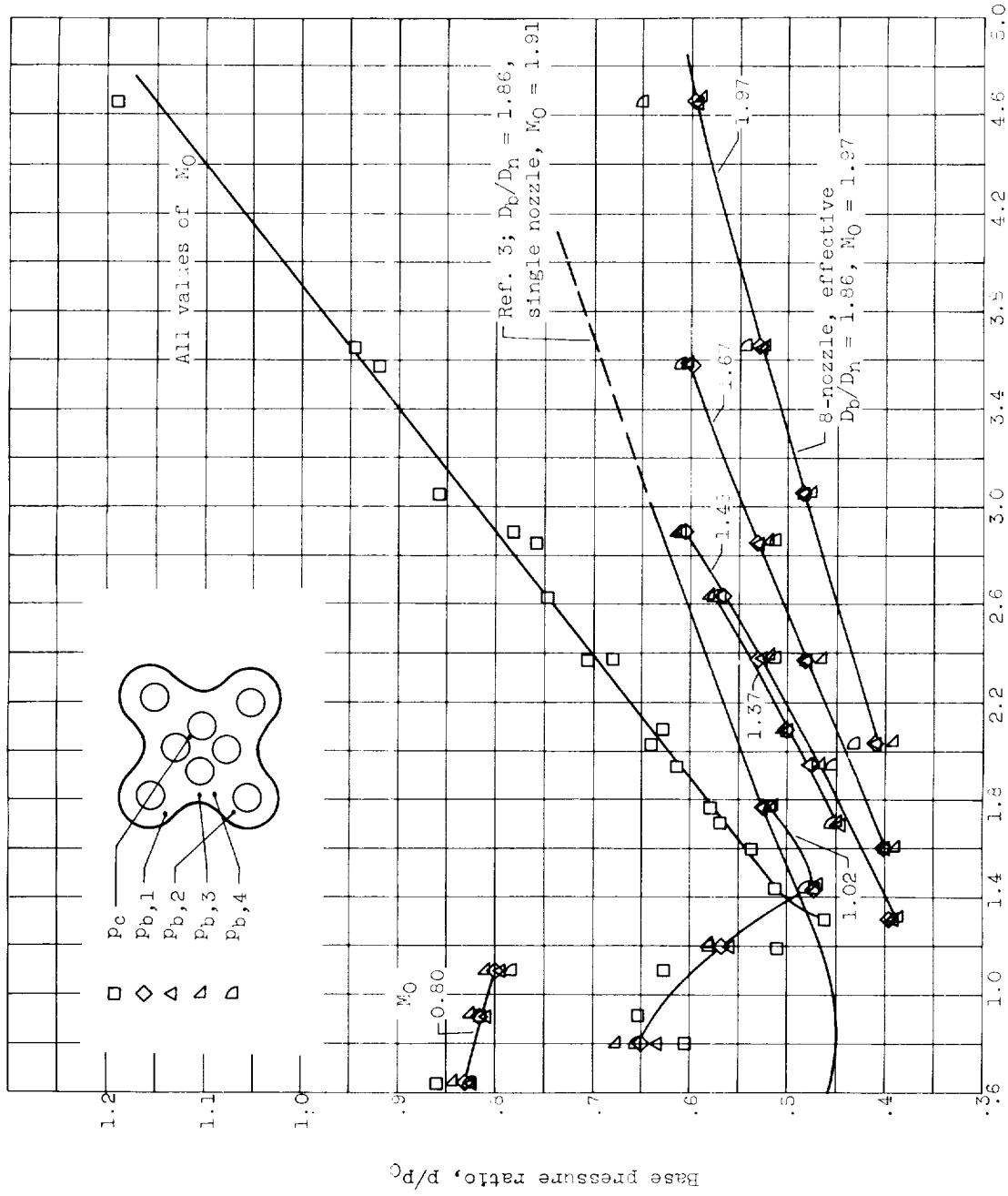

Figure 7. - Base pressures for various flight Mach numbers. Exhausters off.

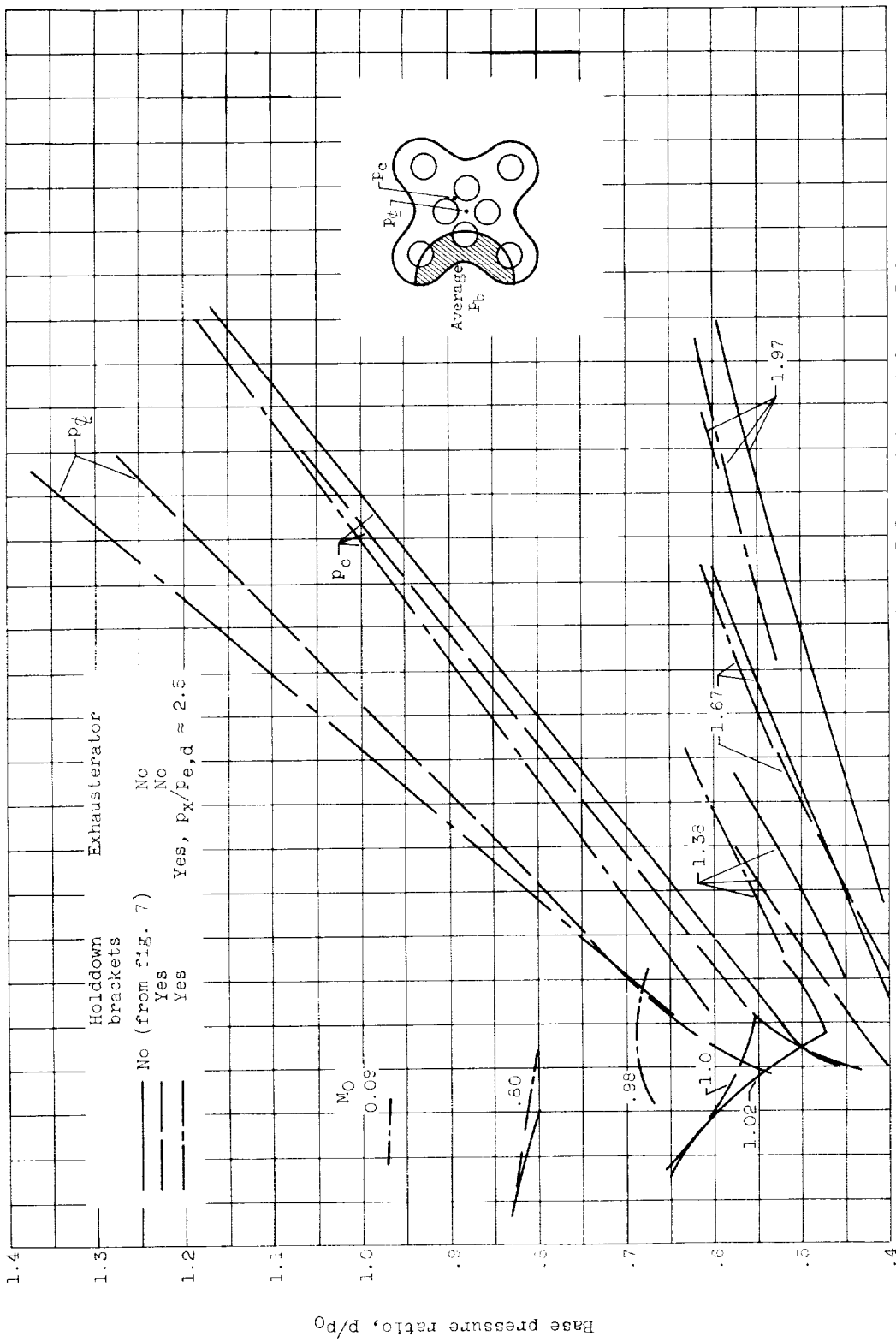

Figure 8. - Base pressure ratio comparison.

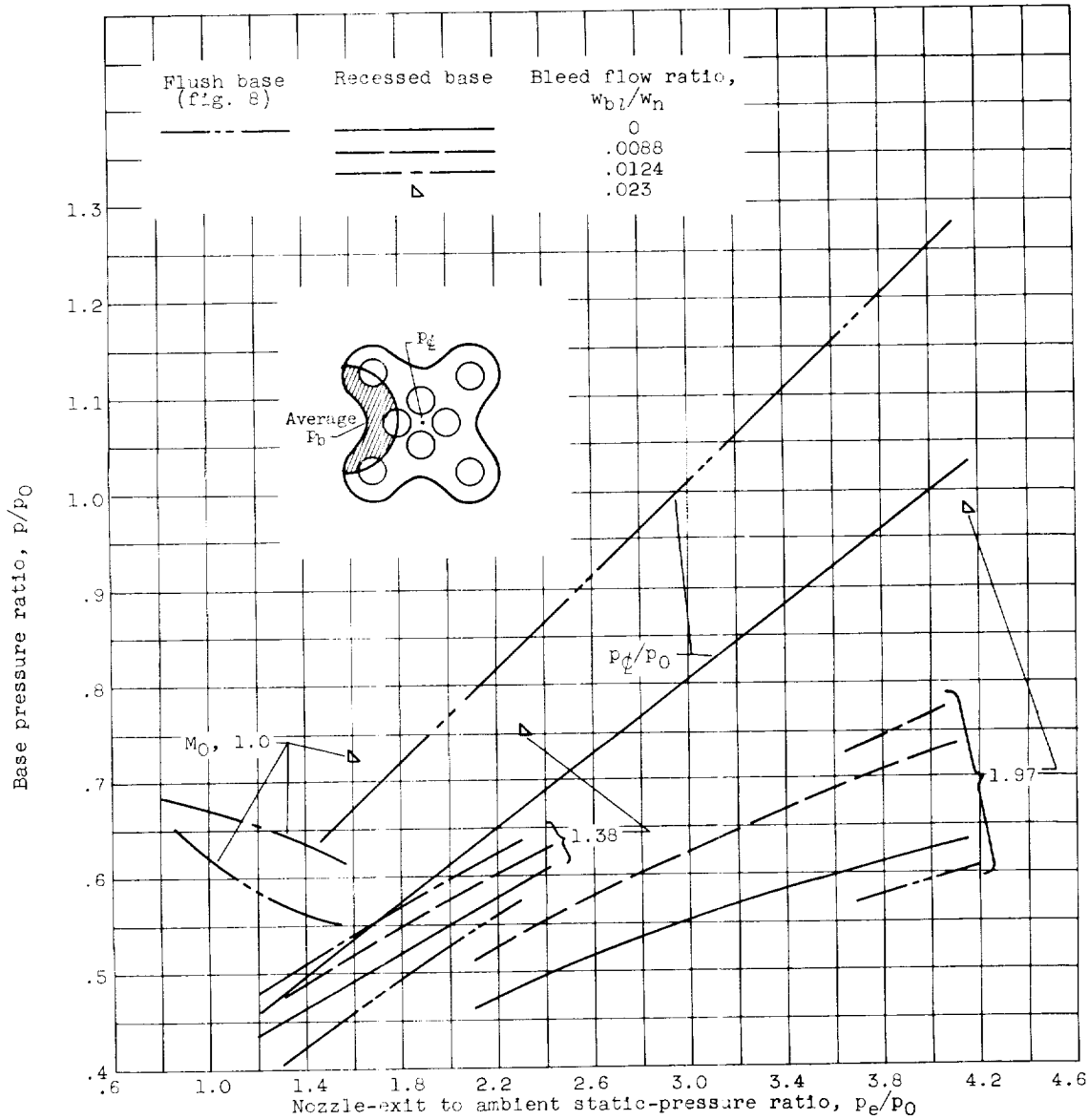

Figure 9. - Effect of bleed flow on base pressure. Recessed base, exhausterators off, and holddown brackets on.

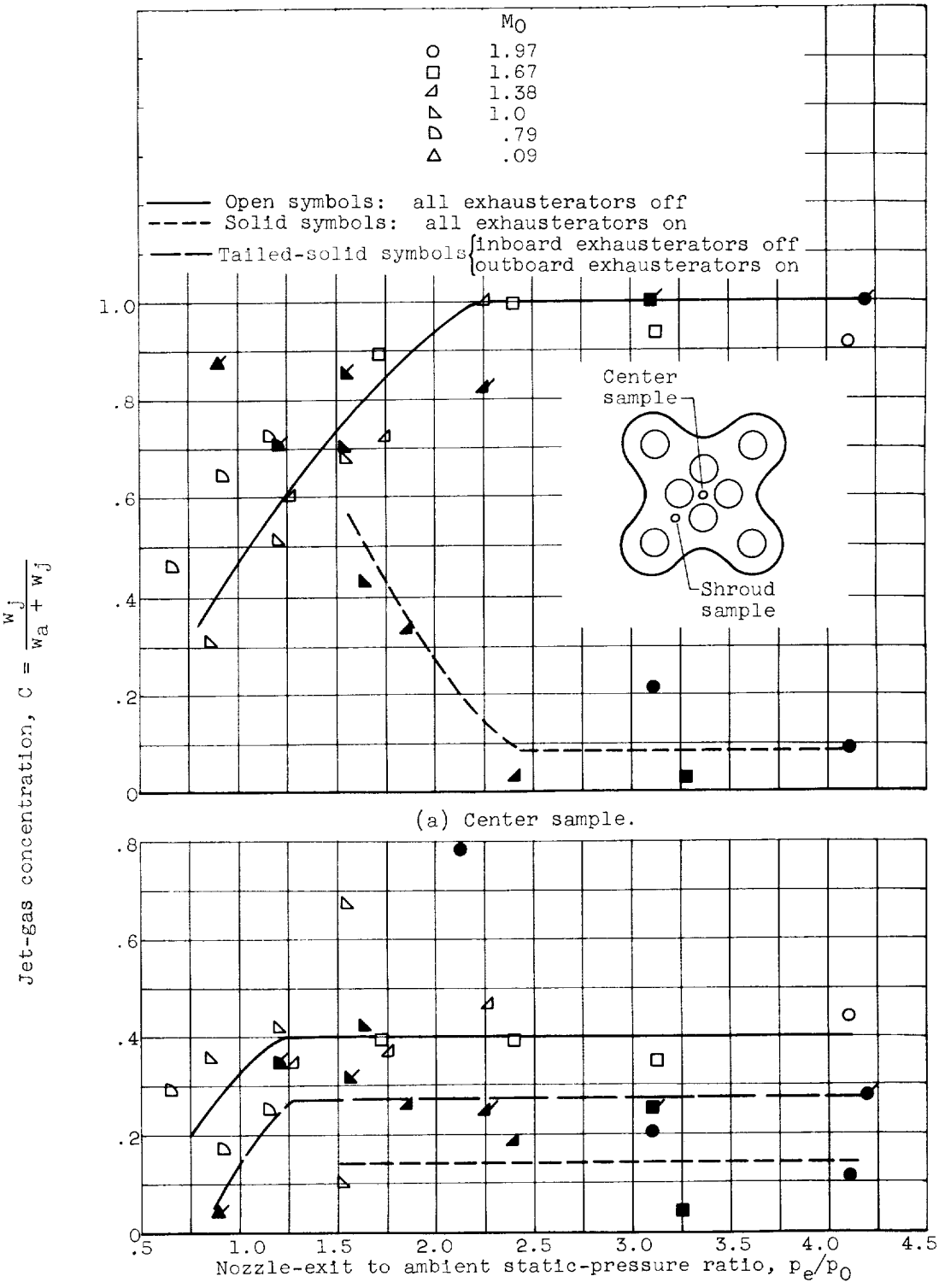

(a) Center sample.

(b) Shroud sample.

Figure 10. - Measurements of jet-gas concentrations in the base.

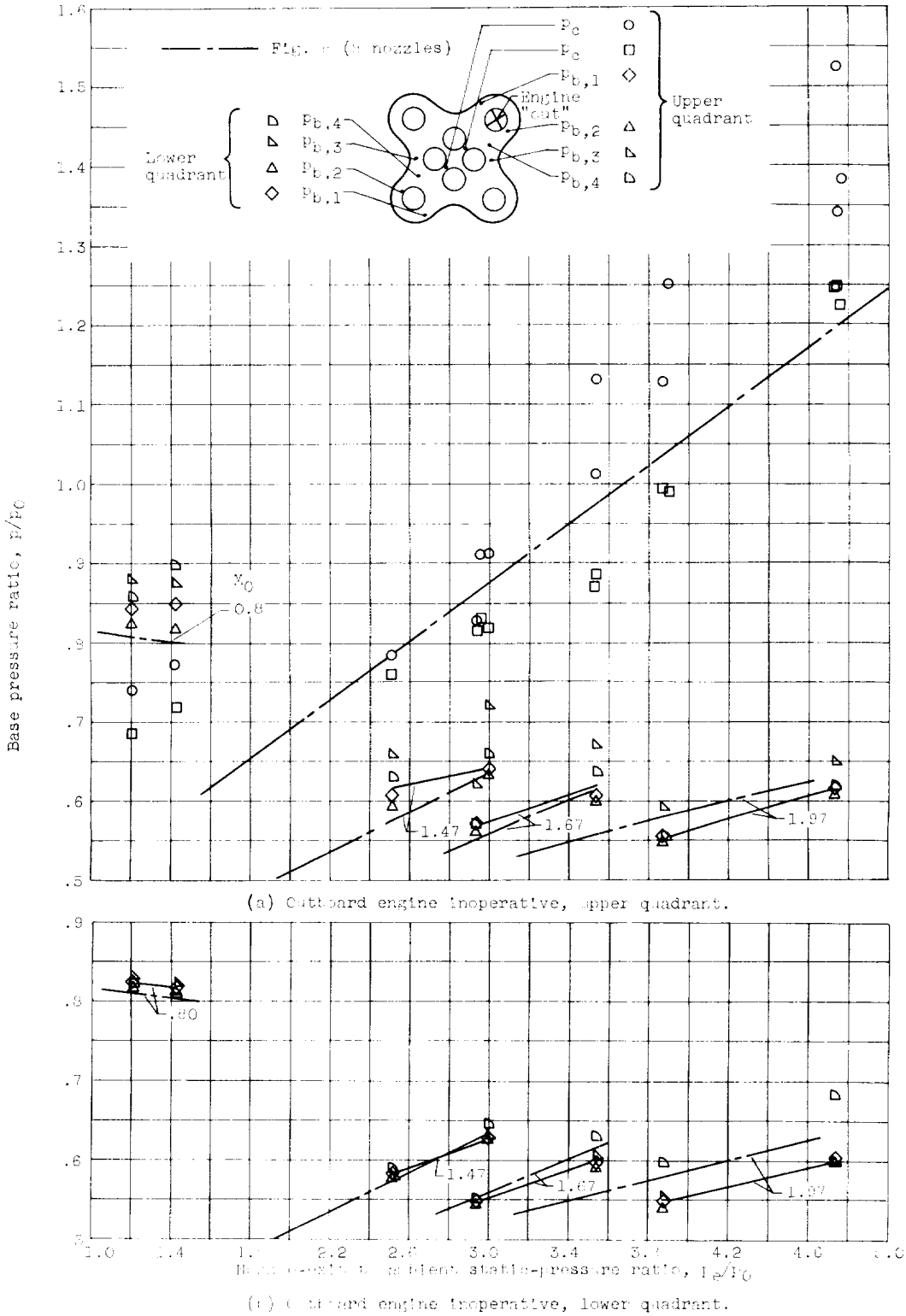

(a) Outboard engine inoperative, upper quadrant.

(b) Outboard engine inoperative, lower quadrant.

Figure 11. - Effect of inoperative engine on base pressure. Holddown brackets installed. $p_x/p_{c,1} = 2.4$.

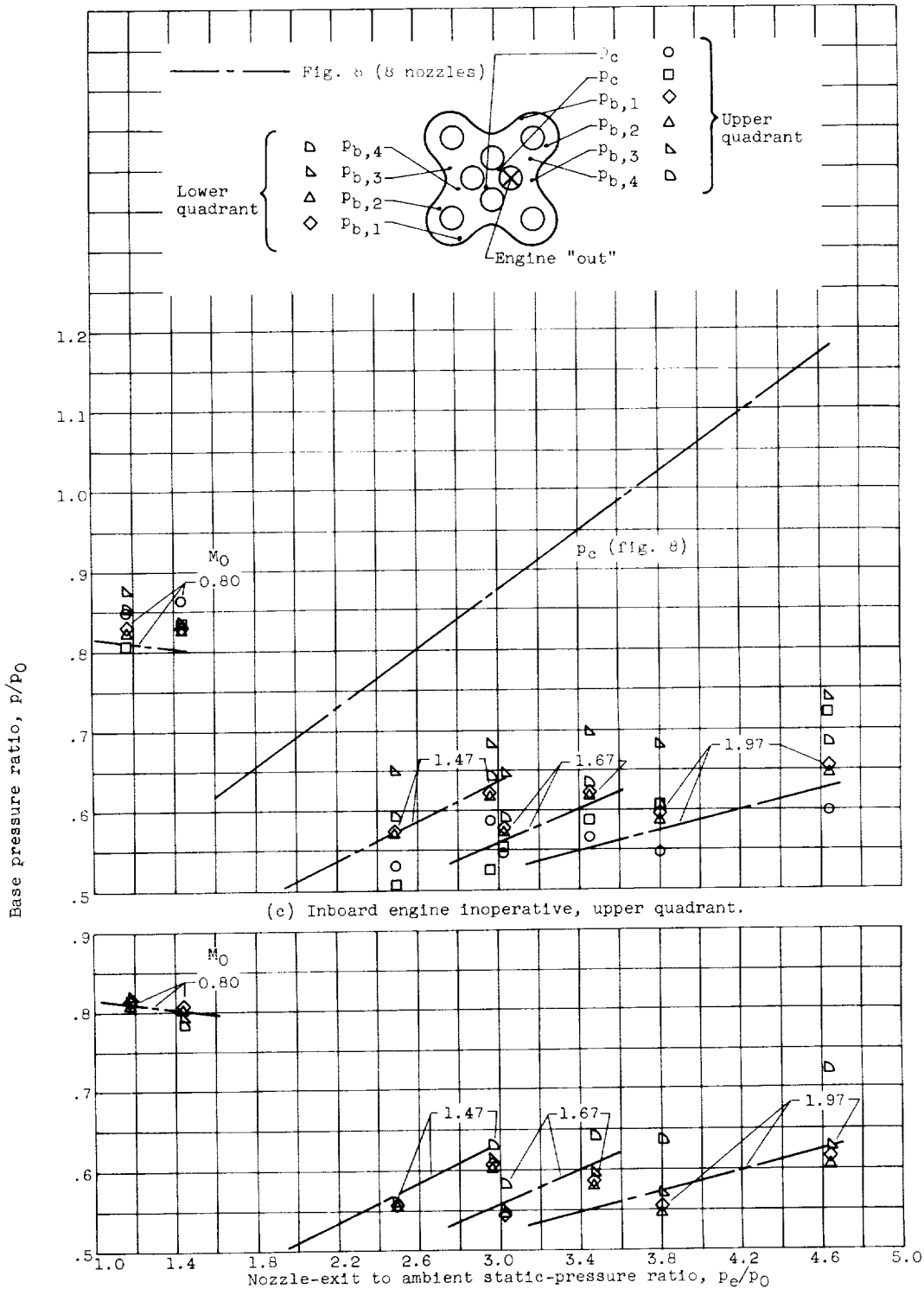

(c) Inboard engine inoperative, upper quadrant.

(d) Inboard engine inoperative, lower quadrant.

Figure 11. - Concluded. Effect of inoperative engine on base pressure. Hold-down brackets installed. $p_x/p_{e,d} \approx 2.4$.

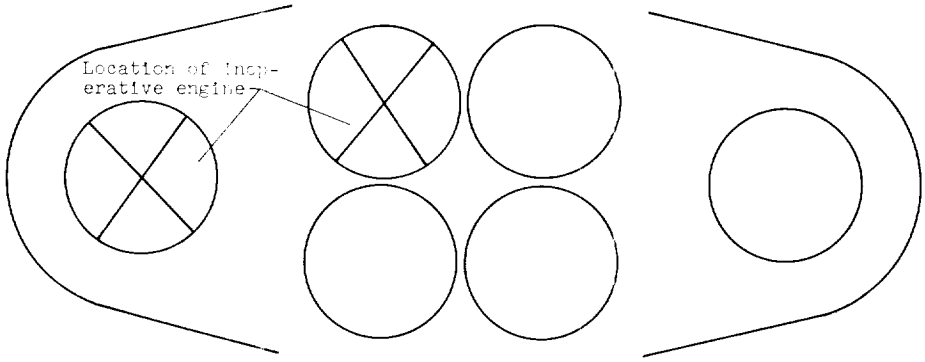

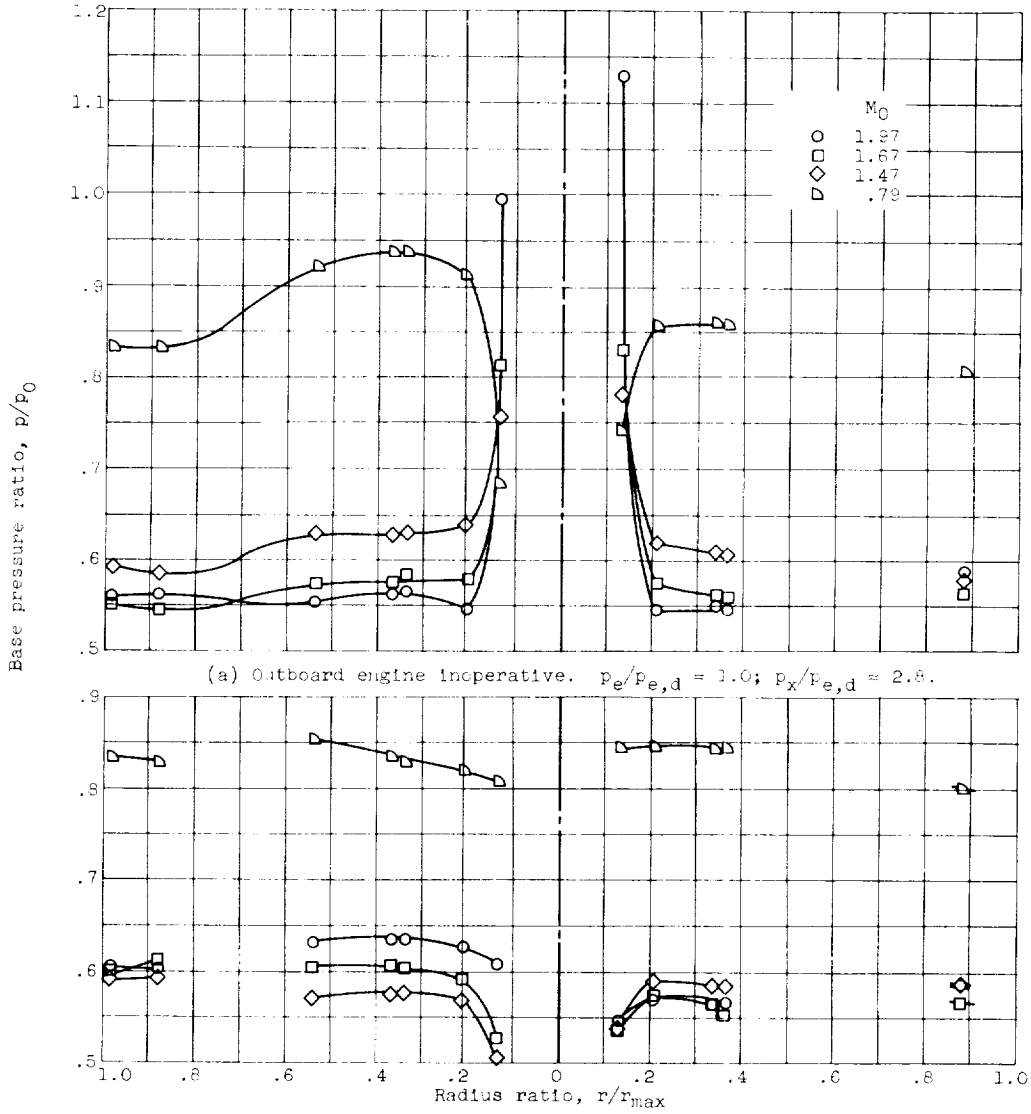

(a) Outboard engine inoperative. $p_e/p_{e,d} = 1.0$; $p_x/p_{e,d} \approx 2.8$.

(b) Inboard engine inoperative. $p_e/p_{e,d} = 1.0$; $p_x/p_{e,d} \approx 2.1$.

Figure 12. - Base diagonal pressure distributions with various inoperative engines.